

Relaxation of Ne^{1+} $1s^0 2s^2 2p^6$ *np* produced by resonant excitation of an ultraintense ultrafast x-ray pulse

Jie Yan(闫杰), Yanpeng Liu(刘彦鹏), Yong Hou(侯永), Cheng Gao(高城), Jianhua Wu(吴建华), Jiaolong Zeng(曾交龙), and Jianmin Yuan(袁建民)

Citation: Chin. Phys. B, 2023, 32 (**6**): 063101. DOI: 10.1088/1674-1056/acc3fa
Journal homepage: http://cpb.iphy.ac.cn; http://iopscience.iop.org/cpb

What follows is a list of articles you may be interested in

Theoretical study of electron-impact broadening for highly charged Ar XV ion lines

Chao Wu(吴超), Xiang Gao(高翔), Yu-Hao Zhu(朱宇豪), Xiao-Ying Han(韩小英), Bin Duan(段斌),Ju Meng(孟举), Song-Bin Zhang(张松斌), Jun Yan(颜君), Yong Wu(吴勇), and Jian-Guo Wang(王建国)

Chin. Phys. B, 2023, 32 (**5**): 053101. DOI: 10.1088/1674-1056/acb769

Effect of conical intersection of benzene on non-adiabatic dynamics

Duo-Duo Li(李多多) and Song Zhang(张嵩)

Chin. Phys. B, 2022, 31 (**8**): 083103. DOI: 10.1088/1674-1056/ac5607

Ab initio investigation of excited state dual hydrogen bonding interactions and proton transfer mechanism for novel oxazoline compound

Yu-Sheng Wang(王玉生), Min Jia(贾敏), Qiao-Li Zhang(张巧丽), Xiao-Yan Song(宋晓燕), Da-Peng Yang(杨大鹏)

Chin. Phys. B, 2019, 28 (**10**): 103105. DOI: 10.1088/1674-1056/ab4042

Lattice structures and electronic properties of WZ-$CuInS_2$/WZ-CdS interface from first-principles calculations

Hong-Xia Liu(柳红霞), Fu-Ling Tang(汤富领), Hong-Tao Xue(薛红涛), Yu Zhang(张宇), Yu-Wen Cheng(程育汶), Yu-Dong Feng(冯煜东)

Chin. Phys. B, 2016, 25 (**12**): 123101. DOI: 10.1088/1674-1056/25/12/123101

Time-dependent density functional theoretical studies on the photo-induced dynamics of an HCl molecule encapsulated in C_{60} under femtosecond laser pulses

Liu Dan-Dan (刘丹丹), Zhang Hong (张红)

Chin. Phys. B, 2013, 22 (**10**): 103103. DOI: 10.1088/1674-1056/22/10/103103

RAPID COMMUNICATION

Relaxation of Ne^{1+} $1s^02s^22p^6np$ produced by resonant excitation of an ultraintense ultrafast x-ray pulse

Jie Yan(闫杰)[1], Yanpeng Liu(刘彦鹏)[2], Yong Hou(侯永)[1], Cheng Gao(高城)[1,†], Jianhua Wu(吴建华)[1,‡], Jiaolong Zeng(曾交龙)[1,3], and Jianmin Yuan(袁建民)[1,4]

[1] *Department of Physics, College of Science, National University of Defense Technology, Changsha* 410073, *China*
[2] *State Key Laboratory of Laser Interaction with Matter, Northwest Institute of Nuclear Technology, Xi'an* 710000, *China*
[3] *College of Science, Zhejiang University of Technology, Hangzhou* 310023, *China*
[4] *Graduate School of China Academy of Engineering Physics, Beijing* 100193, *China*

(Received 10 January 2023; revised manuscript received 4 March 2023; accepted manuscript online 14 March 2023)

The creation and relaxation of double K-hole states $1s^02s^22p^6np$ ($n \geq 3$) of Ne^{1+} in the interaction with ultraintense ultrafast x-ray pulses are theoretically investigated. The x-ray photon energies are selected so that x-rays first photoionize $1s^22s^22p^6$ of a neon atom to create a single K-hole state of $1s2s^22p^6$of Ne^{1+}, which is further excited resonantly to double K-hole states of $1s^02s^22p^6np$ ($n \geq 3$). A time-dependent rate equation is used to investigate the creation and relaxation processes of $1s^02s^22p^6np$, where the primary microscopic atomic processes including photoexcitation, spontaneous radiation, photoionization and Auger decay are considered. The calculated Auger electron energy spectra are compared with recent experimental results, which shows good agreement. The relative intensity of Auger electrons is very sensitive to the photon energy and bandwidth of x-ray pulses, which could be used as a diagnostic tool for x-ray free electron laser and atom experiments.

Keywords: hollow atoms, x-ray resonant excitation, relaxation

PACS: 31.15.ag, 32.80.Aa **DOI:** 10.1088/1674-1056/acc3fa

1. Introduction

Transient atomic states are critical in the fields of atoms and molecules,[1–4] clusters[5,6] and solids.[7,8] They pose a significant challenge to researchers because of their very short lifetime.[9] With the application of x-ray free electron laser (XFEL) such as the Linac Coherent Light Source (LCLS),[10] European XFEL[11] and Spring-8 Angstrom Compact free electron Laser (SACLA),[12] ultrafast (few to hundreds of femtoseconds (fs)) and ultraintense ($\sim 10^{18}$–10^{22} W/cm^2) x-ray pulses are provided. XFEL interacts primarily with inner-shell electrons leaving multiple core-holes in the atom or molecule.[13–15] Single and double core-hole (SCH/DCH) states could be created readily due to the extreme brightness of XFEL and many studies on SCH and DCH states in the interaction with XFEL have been performed in the past decade.[16–19]

SCH and DCH states are usually created by x-ray photoionization when irradiated by XFEL. However, resonant excitation is a much more efficient channel than photoionization because the resonant excitation rate is generally several times higher. Resonant excitation actually plays a crucial role on the ionization kinetics. Although resonant excitation in long wavelength regions has been well studied,[20] there has been increasing interest in x-ray regions in the recent decade.[2,21–24] For example, resonant excitation can efficiently enhance ionization in complex atomic systems such as Kr and Xe in the interaction with XFEL.[2,23] Even for relatively simple atoms such as Ar and Ne, resonant excitation can significantly affect ionization kinetic pathways and charge state distribution.[21,23,24] However, these resonant excitation studies are mainly focused on SCH states. For DCH states, big challenges exist because of the shorter lifetime and more complicated atomic structure. Recently, Mazza *et al.*[25] experimentally investigated the formation and relaxation of DCH states of neon on European XFEL.[11] In the experiment, x-ray photon energy was tuned to ionize one 1s electron and then resonantly excite the other 1s electron to np orbitals. As a result, $1s^02s^22p^6np$ were effectively created and the relaxation process was recorded using Auger electron spectra. However, the details of the formation and relaxation of $1s^02s^22p^6np$ are still not well understood.

In this work, we used a time-dependent rate equation to simulate the production and relaxation processes of $1s^02s^22p^6np$ in the interaction with ultraintense ultrafast x-ray pulses. The dominant microscopic atomic processes including resonant photoexcitation and deexcitation, photoionization, as well as Auger decay, are considered in this calculation. Resonant transition channels which are crucial for the level pop-

†Corresponding author. E-mail: gaocheng@nudt.edu.cn
‡Corresponding author. E-mail: jianhuawu@nudt.edu.cn

© 2023 Chinese Physical Society and IOP Publishing Ltd

ulation of DCH states are studied. Auger electron emission spectra are calculated using the atomic level populations obtained from the rate equation. The relative intensity of Auger electrons from $1s^02s^22p^6np$ is studied in detail, showing that it is very sensitive to the photon energy and bandwidth of the x-ray pulses.

2. Theoretical method

To understand the atomic level population kinetics interacting with XFEL, a master equation approach is primarily recommended.[26,27] However, a rate equation approximation is commonly used instead[15,28–30] because of the relatively low temporal coherence of x-ray pulses in self-amplified spontaneous emission (SASE) mode.[31,32] The details of a rate equation approach can be found elsewhere,[33] but a brief introduction is given here. The population n_i of atomic level i is determined using the following

$$\frac{\mathrm{d}n_i}{\mathrm{d}t} = \sum_{j\neq i}^{N_\mathrm{L}} n_j R_{ji} - n_i \sum_{j\neq i}^{N_\mathrm{L}} R_{ij}, \tag{1}$$

where R_{ij} and R_{ji} represent the depopulating and populating rates between levels i and j, respectively, and N_L is the total number of energy levels considered in the calculation. In this work, contributions to the rate from photoexcitation and deexcitation, photoionization and Auger decay processes are considered.

The intensity of XFELs has a Gaussian profile with respect to space, time and photon energy, which is expressed as follows:

$$I_{h\nu}(r,t) = I_0\, \mathrm{e}^{-\ln 2(\frac{r}{\Delta})^2}\, \mathrm{e}^{-\ln 2(\frac{t}{\tau})^2} \sqrt{\frac{\ln 2}{\pi\Gamma^2}}\, \mathrm{e}^{-\ln 2(\frac{h\nu-h\nu_0}{\Gamma})^2}, \tag{2}$$

where I_0 is the peak intensity in W/cm^2 and $h\nu_0$ is the central photon energy of the x-ray pulse. Δ, τ and Γ are the half width at half maximum (HWHM) of the Gaussian profile of the x-ray pulse on the distribution of space, time and photon energy, respectively. The XFEL pulses at the SASE mode are usually spiky and thus the x-ray pulses are partially temporal coherent.[34] The envelope of these spikes in the time and frequency domain can be approximated by Gaussian functions with an averaged duration and bandwidth.[28] The populations in experiments are obtained by averaging over many shots which eliminate the influences of spikes in the x-ray pulses. Therefore it is reasonable to assume Gaussian distribution functions for the x-ray pulse intensity.

The resonant excitation rate from levels i to j can be expressed as follows:

$$R_{ij}^{\mathrm{re}} = \int \frac{I_{h\nu}}{h\nu}\sigma_{ij}(h\nu)\,\mathrm{d}(h\nu), \tag{3}$$

where $\sigma_{ij}(h\nu) = \frac{\pi h e^2}{m_\mathrm{e}c} f_{ij} S(h\nu)$ is the absorption cross section with f_{ij} being the absorption oscillator strength and $S(h\nu)$ being the line shape.

A complete set of atomic data including energy levels, oscillator strength, photoionization cross section and Auger decay rate is obtained using FAC code,[35] which solves the Dirac equation to obtain the orbital wavefunctions. A distorted wave approximation is used to treat continuum atomic processes. Configuration interaction and relativistic effects are considered in this calculation. Note that double Auger decay rate of $1s^02s^22p^6np$ is about one order of magnitude smaller than the single Auger decay rate.[36] Therefore only single Auger decays are included in the this work. In the present calculation, the neon atoms are populated initially in the ground state of $1s^22s^22p^6$. The configurations of the ground, singly excited from valence shells, SCH and DCH states are included. Take Ne^{1+} as an example. The following configurations are considered: $1s^22s^22p^5$, $1s^22s2p^6$, $1s^22s^22p^43l$, $1s^22s2p^53l$, $1s^22p^63l$, $1s2s^22p^6$, $1s2s^22p^53l$, $1s2s2p^63l$, $1s^02s^22p^6nl$ ($n = 3-8, l = 0,1,2,\ldots,n-1$). The rate equations are solved in the different positions of the laser spot to obtain the populations. The calculated populations after temporal and spatial averaging are used to compare with the experimental results.

In the recent experiment,[25] the x-ray photon energies are tuned to first photoionize one 1s electron and then excite resonantly the other 1s electron of neon to an np orbital. Such a process can be simply expressed as $1s^22s^22p^6 + h\nu \rightarrow 1s2s^22p^6 + e^-$ and $1s2s^22p^6 + h\nu \rightarrow 1s^02s^22p^6np$ ($n \geq 3$). Photoexcitation and photoionization rates of these processes are crucial for the production of $1s^02s^22p^6np$. Because of the extremely non-equilibrium properties of hole atoms,[37,38] obtaining precise transition data is difficult. In this work, the R-matrix method is used to calculate the transition data near the K-edge of $1s2s^22p^6$ of Ne^{1+}, which is a very effective approximation to treat the photon– and electron–atom interactions.[39,40] The details of the R-matrix calculation are similar to our previous work.[41] In summary, 44 energy terms are chosen as target states which belong to the SCH states of Ne^{2+}, i.e., $1s2s^22p^5$, $1s2s2p^6$, $1s2s^22p^43p$, $1s2s2p^53p$ and $1s2p^63p$. Five real (1s, 2s, 2p, 3s, 3p) and four pseudo-orbitals ($\overline{3}$d, $\overline{4}$s, $\overline{4}$p, $\overline{4}$d), which are obtained using the CIV3 code,[42] are employed to construct wavefunctions of these target states. The calculated ionization threshold of $1s2s^22p^6$ is 994.3 eV which agrees well with the experimental value of $\sim$ 993 eV.[43]

3. Results and discussion

The calculated photoabsorption cross section of $1s2s^22p^6$ of Ne^{1+} near the K-edge, which is convolved with the total width (natural and Auger width), is illustrated in Fig. 1(a). The dashed line represents the x-ray profile with a center photon energy of 991 eV and bandwidth of 4.5 eV (HWHM)

which is consistent with the reported x-ray bandwidth of 0.1%.[25] The photon energy (991 eV) corresponds to the transition energy of $1s2s^22p^6 \rightarrow 1s^02s^22p^65p$. However, the x-ray can also effectively excite nearby transition lines of $1s2s^22p^6 \rightarrow 1s^02s^22p^64p/6p/7p/\cdots$. The transition energy of $1s2s^22p^6 \rightarrow 1s^02s^22p^63p$ is approximately 982 eV, which overlaps with the edge of the x-ray profile. Because of the large absorption oscillator strength, the photoexcitation rate of $1s2s^22p^6 \rightarrow 1s^02s^22p^63p$ should play a role. The x-ray profile also includes the photoionization region, so $1s2s^22p^6 + h\nu \rightarrow 1s^02s^22p^6 + e^-$ could occur. The corresponding photoabsorption rates of different channels from $1s2s^22p^6$ at the center of the laser spot are shown in Fig. 1(b). The $1s \rightarrow 3p$, $1s \rightarrow 4p$ and $1s \rightarrow \varepsilon p$ rates are larger than $1s \rightarrow 5p$, although the x-ray center photon energy 991 eV corresponds to the $1s \rightarrow 5p$ transitions. Furthermore, the rate of $1s \rightarrow 4p$ is larger than that of $1s \rightarrow 3p$ whereas both are smaller than the photoionization rate.

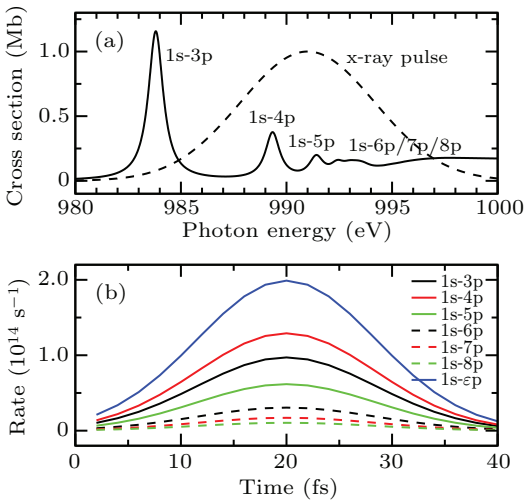


Fig. 1. (a) Photoabsorption cross section near the K-edge of $1s2s^22p^6$ of Ne^{1+}. The dashed-line represents an x-ray pulse with center photon energy $h\nu_0 = 991$ eV and bandwidth $\Gamma = 4.5$ eV. (b) The corresponding photoexcitation and photoionization rate of different transition channels at the center ($r = 0$ μm) of the laser spot. For the x-ray pulse, $\Delta = 1$ μm, $\tau = 10$ fs, and the maximal laser intensity $I_0 = 1 \times 10^{18}$ W/cm^2 reaches at $t = 20$ fs.

Photoabsorption rates determine the level populations shown in Fig. 2. The populations of DCH states increase quickly at the center of laser spot ($r = 0$) as shown in Fig. 2(a), reach their maximum at approximately 7 fs, and then deplete at about 15 fs. The population of $1s^02s^22p^64p$ is the largest with a maximum value of about 1.3%. The population of $1s^02s^22p^6$ is smaller than that of $1s^02s^22p^63p$ and $1s^02s^22p^64p$. However, the photoionization rate is larger than the resonant absorption rate (as shown in Fig. 1(a)). This is due to Auger decay rate. The Auger rate of $1s^02s^22p^6$ is about 1.9×10^{15} s^{-1},[41,44,45] which is larger than that of $1s^02s^22p^6np$ ($\sim 1\times10^{15}$ s^{-1}).[36,46] Therefore, the population of $1s^02s^22p^6$ is smaller than that of $1s^02s^22p^63p/4p$. The maximal populations of the DCH states become smaller at the outer positions of the laser spot. For example, the maximal population of $1s^02s^22p^64p$ is $\sim 1.3\%$ at the center of the laser spot, $\sim 0.8\%$ at $r = 1$ μm and $\sim 0.15\%$ at $r = 2$ μm. The outer the position in the laser spot, the later the population reaches its maximum value. The population profile gets wider from the innermost to the outermost positions. This is mainly due to a decrease in laser intensity from the inner to outer positions, resulting in a consequent decrease in the photoexcitation rate. In the interaction with x-rays, the neon atoms are depleted quickly. Consequently $1s2s^22p^6$ of Ne^{1+} are populated which are further transferred into $1s^02s^22p^6$ of Ne^{2+} by photoionization and $1s^02s^22p^6np$ by resonant photoexcitation. The population of Ne^{2+} is depleted due to the large Auger decay rate. As a result the population is transferred to the SCH states of Ne^{3+} which further decays into Ne^{4+}. Different charge states are created in such a way in the interaction of ultrafast ultraintense x-ray with neon.

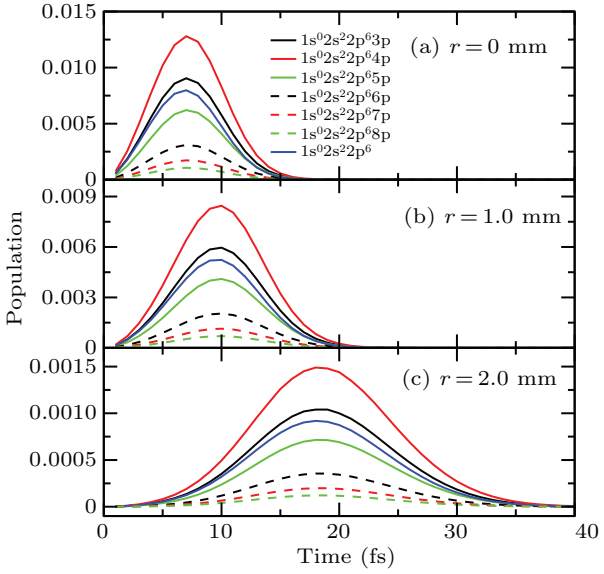


Fig. 2. Population evolution of $1s^02s^22p^6np$ and $1s^02s^22p^6$ in laser spot of (a) $r = 0$ μm, (b) $r = 1.0$ μm, and (c) 2.0 μm. The x-ray parameters are the same as those shown in Fig. 1.

Auger electron spectra are important because they reveal information about the ionization processes.[1] In this study, the intensity of Auger electrons is calculated using

$$I(\varepsilon) = \sum_{ji} n_j A_{ji} \frac{\gamma/\pi}{(\varepsilon - \varepsilon_0)^2 + \gamma^2}, \tag{4}$$

where n_j is the population of hole state j, A_{ji} is the Auger decay rate, ε_0 is the energy of Auger electrons, and γ represents the spectral width (HWHM) which takes a Lorentzian line shape.

Figure 3 shows the calculated Auger electron emission spectra. These theoretical spectra are obtained by temporal and spatial averaging over the duration and laser spot.[15,47] Auger electrons are obtained from the decay of $1s^02s^22p^6np$ of Ne^{1+} and $1s^02s^22p^6$ of Ne^{2+} in the electron energy range of 865–890 eV, as shown in Fig. 3(a). The peaks at electron energy of $\sim$ 880 eV are contributed mainly by the decay of

$1s^02s^22p^63p \rightarrow 1s2s^22p^43p + e^-$ and the peak at $\sim$ 875 eV is caused by $1s^02s^22p^64p \rightarrow 1s2s^22p^44p + e^-$. The peaks at $\sim$ 870 eV are contributed by $1s^02s^22p^6np$ ($n \geq 5$) and $1s^02s^22p^6$. The theoretical spectra are convolved with an instrumental resolution of 1.05 eV (HWHM),[25] and normalized to the experimental peak at $\sim$ 870 eV to compare with the experimental spectra (Figs. 3(b) and 3(c)). The relative intensity is very sensitive to the x-ray photon energy at a particular x-ray bandwidth, as shown in Fig. 3(b). The intensities of Auger electrons from $1s^02s^22p^63p$ and $1s^02s^22p^64p$ are larger than the corresponding experimental results at x-ray center photon energy of 990 eV (black solid line). With the increase in x-ray photon energy, both intensities decrease. The best agreement with the experimental results is achieved for the x-ray photon energy of 991 eV, which is consistent with the reported value of 991±0.5 eV.[25] Figure 3(c) shows the relative intensity for a fixed x-ray photon energy of 991 eV and variable bandwidth. The sensitivity to the bandwidth is also observed. However, as the bandwidth increases, the intensities of $1s^02s^22p^63p$ and $1s^02s^22p^64p$ show an opposite trend, with the former increasing while the latter decreasing. This behavior differs from that shown in Fig. 3(b). For a fixed bandwidth (Fig. 3(b)), as the x-ray photon energy increases from 990 eV to 992 eV, the photons that can excite $1s \rightarrow 3p$ and $1s \rightarrow 4p$ decrease and thus both populations of $1s^02s^22p^63p$ and $1s^02s^22p^64p$ decrease. For a fixed x-ray photon energy (Fig. 3(c)), as the x-ray bandwidth increases from 4.0 eV to 6.0 eV, the photons that can excite $1s \rightarrow 4p$ decrease while the photons that can excite $1s \rightarrow 3p$ increase. Therefore the populations of $1s^02s^22p^63p$ and $1s^02s^22p^64p$ exhibit opposing changing characteristics.

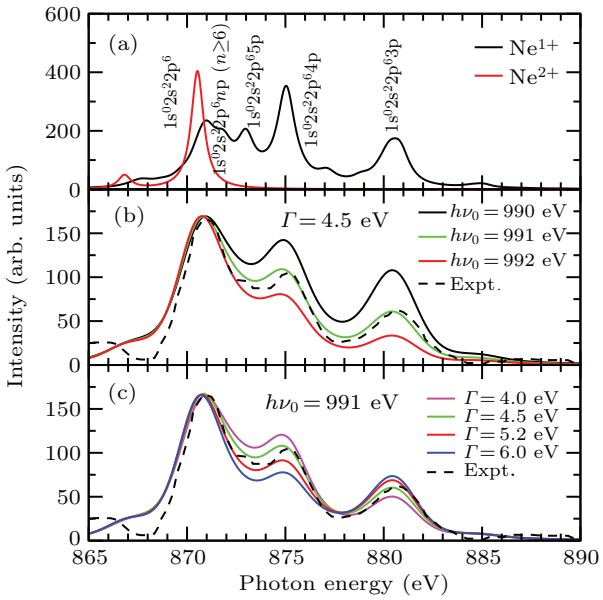


Fig. 3. Auger electron emission spectra in interaction with x-ray pulses. In panel (a), Auger electron emission spectra contributed by $1s^02s^22p^6np$ of Ne^{1+} and $1s^02s^22p^6$ of Ne^{2+} are shown. The x-ray pulse parameters are the same as those shown in Fig. 1. In panel (b), the x-ray bandwidth of 4.5 eV is fixed and the x-ray center photon energy is variable. In panel (c), the x-ray center photon energy of 991 eV is fixed and the x-ray bandwidth is variable. Other x-ray pulse parameters are the same as those shown in Fig. 1. The theoretical spectra are shifted by 2.2 eV to the lower electron energy range to fit the experimental spectra.

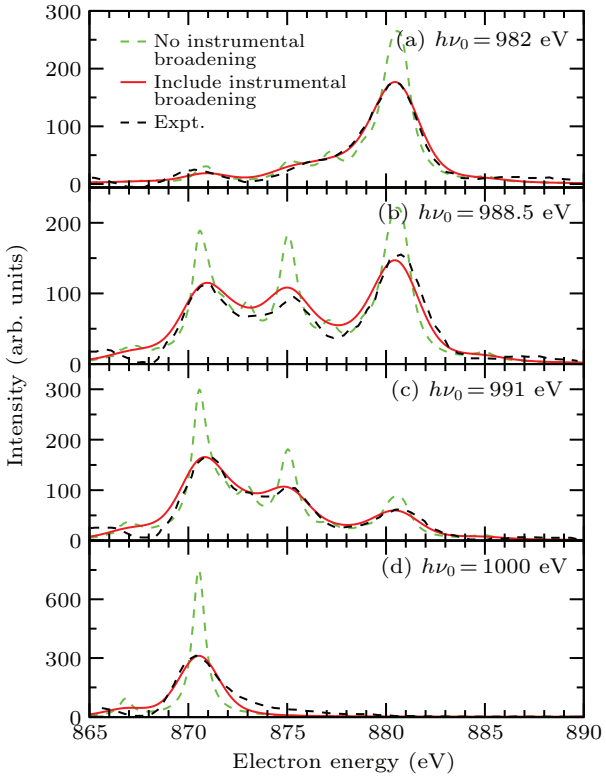


Fig. 4. Auger electron spectra in interaction with x-ray pulses with a variable center photon energy of (a) 982 eV, (b) 988.5 eV, (c) 991 eV and (d) 1000 eV. The black dashed lines represent the experimental results.[25] The red solid lines represent the theoretical spectra with instrumental broadening (1.05 eV) included and the green dashed lines are with no instrumental broadening included. Other x-ray pulse parameters are the same as those shown in Fig. 1.

For systematical investigations, Fig. 4 compares the theoretical and experimental results for a variable x-ray photon energy of (a) 982 eV, (b) 988.5 eV, (c) 991 eV and (d) 1000 eV, respectively. At an x-ray photon energy of 982 eV (Fig. 4(a)), the resonant excitation rate of $1s2s^22p^6 + h\nu \rightarrow 1s^02s^22p^63p$ is the largest which is about one order of magnitude larger than that of $1s2s^22p^6 + h\nu \rightarrow 1s^02s^22p^64p$. The Auger decay of $1s^02s^22p^63p$ into the fine structure levels of $1s2s^22p^43p$ forms the peaks near the electron energies of 875 eV, 877 eV, 880 eV and 885 eV. The relatively weak peaks near the electron energy of 871 eV are from the shakeup process of $1s^02s^22p^63p \rightarrow 1s2s^22p^44p + e^-$. The theoretical spectra are broadened and agree well with the experimental results after considering the instrumental broadening effect.[25] Figure 4(b) shows the case for the x-ray photon energy of 988.5 eV which corresponds to the transition energy of $1s2s^22p^6 + h\nu \rightarrow 1s^02s^22p^64p$. However, it is interesting to find that the largest Auger electron intensity is from $1s^02s^22p^63p$. The photoexcitation rate of $1s \rightarrow 3p$ is larger than that of $1s \rightarrow 4p$ by 70% because of the larger absorption cross section of $1s \rightarrow 3p$ (as shown in Fig. 1). Due to the bandwidth of x-ray pulses, $1s^02s^22p^6np$ ($n \geq 5$) and $1s^02s^22p^6$ are also populated and the Auger decay

of these DCH states form the peaks near the electron energy of 870 eV. The Auger electron emission spectra are very different as the x-ray photon energy increasing from 988.5 eV to 991 eV. The strongest electron emission spectra are from the decay of $1s^02s^22p^63p$ at $h\nu_0 = 988.5$ eV while they are the weakest at $h\nu_0 = 991$ eV. These characteristics clearly demonstrate the sensitivity of Auger electron emission spectra on the x-ray photon energy when they are located in the resonant excitation regions. At the highest x-ray photon energy of 1000 eV (Fig. 4(d)), no resonant absorption can be excited while only photoionization occurs. Therefore only $1s^02s^22p^6$ is created and its decay forms the emission peak at ~ 870 eV.

4. Conclusion

In summary, the formation and relaxation of neon *K*-shell DCH states in the interaction with ultraintense ultrafast x-ray pulses are theoretically investigated. Particular attention is paid to $1s^02s^22p^6np$, which are resonantly excited from $1s2s^22p^6$. The population evolution of atomic hole states is studied using a rate equation approach. The results show that resonant excitation could efficiently populate DCH states. The Auger electron emission spectra are investigated at different x-ray photon energies ranging from resonant excitation to the photoionization region, and they show significantly different characteristics. These calculations agree well with the experimental results.[25] The Auger electron spectra are very sensitive to the center photon energy and bandwidth of the x-ray pulses when the x-ray photon energy corresponds to a specific resonant excitation. This conclusion could be helpful for lifetime control of hole states.[48]

Acknowledgement

Project supported by the National Natural Science Foundation of China (Grant Nos. 12074430 and 11974423).

References

[1] Young L, Kanter E P, Krässig B, *et al*. 2010 *Nature* **466** 56
[2] Rudek B, Son S K, Foucar L, *et al*. 2012 *Nat. Photon.* **6** 858
[3] Fang L, Hoener M, Gessner O, Tarantelli F, Pratt S T, Kornilov O, Buth C, Gühr M, Kanter E P, Bostedt C, Bozek J D, Bucksbaum P H, Chen M, Coffee R, Cryan J, Glownia M, Kukk E, Leone S R and Berrah N 2010 *Phys. Rev. Lett.* **105** 083005
[4] Rudenko A, Inhester L, Hanasaki K, *et al*. 2017 *Nature* **546** 129
[5] Thomas H, Helal A, Hoffmann K, *et al*. 2012 *Phys. Rev. Lett* **108** 133401
[6] Ziaja B, Wabnitz H, Wang F, Weckert E and Möller T 2009 *Phys. Rev. Lett.* **102** 205002
[7] Vinko S M, Ciricosta O, Cho B I, *et al*. 2012 *Nature* **482** 59
[8] Cho B I, Cho M S, Kim M, *et al*. 2017 *Phys. Rev. Lett.* **119** 075002
[9] Ueda K, Sokell E, Schippers S, *et al*. 2019 *J. Phys. B: At. Mol. Opt. Phys.* **52** 171001
[10] Emma P, Akre R, Arthur J, *et al*. 2010 *Nat. Photon.* **4** 641
[11] Tschentscher T, Bressler C, Grünert J, Madsen A, Mancuso A P, Meyer M, Scherz A, Sinn H and Zastrau U 2017 *Appl. Sci.* **7** 592
[12] Ishikawa T, Aoyagi H, Asaka T, *et al*. 2012 *Nat. Photon.* **6** 540
[13] Berrah N and Fang L 2015 *J. Electron Spectrosc. Relat. Phenom.* **204** 284
[14] Buth C, Liu J C, Chen M H, Cryan J P, Fang L, Glownia J M, Hoener M, Coffee R N and Berrah N 2012 *J. Chem. Phys.* **136** 214310
[15] Gao C, Zeng J L and Yuan J M 2016 *J. Phys. B: At. Mol. Opt. Phys.* **49** 044001
[16] Seddon E A, Clarke J A, Dunning D J, Masciovecchio C, Milne C J, Parmigiani F, Rugg D, Spence J C H, Thompson N R, Ueda K, Vinko S M, Wark J S and Wurth W 2017 *Rep. Prog. Phys.* **80** 115901
[17] Bostedt C, Boutet S, Fritz D M, Huang Z, Lee H J, Lemke H T, Bobert A, Schlotter W F, Turner J J and Williams G J 2016 *Rev. Mod. Phys.* **88** 015007
[18] Young L, Ueda K, Gühr M, *et al*. 2018 *J. Phys. B: At. Mol. Opt. Phys.* **51** 032003
[19] Bostedt C, Bozek J D, Bucksbaum P H, *et al*. 2013 *J. Phys. B: At. Mol. Opt. Phys.* **46** 164003
[20] Johnson P M and Otis C E 1981 *Annu. Rev. Phys. Chem.* **32** 139
[21] Xiang W J, Gao C, Fu Y S, Zeng J L and Yuan J M 2012 *Phys. Rev. A* **86** 061401
[22] Toyota K, Son S K and Santra R 2017 *Phys. Rev. A* **95** 043412
[23] Ho P J, Bostedt C, Schorb S and Young L 2014 *Phys. Rev. Lett.* **113** 253001
[24] LaForge A C, Son S K, Mishra D, Ilchen M, Duncanson S, Eronen E, Kukk E, Wirok-Stoletow S, Kolbasova D, Walter P, Boll R, De Fanis A, Meyer M, Ovcharenko Y, Rivas D E, Schmidt P, Usenko S, Santra R and Berrah N 2021 *Phys. Rev. Lett.* **127** 213202
[25] Mazza T, Ilchen M, Kiselev M D, *et al*. 2020 *Phys. Rev. X* **10** 041056
[26] Li Y Q, Gao C, Dong W P, Zeng J L, Zhao Z X and Yuan J M 2016 *Sci. Rep.* **6** 18529
[27] Cavaletto S M, Buth C, Harman Z, Kanter E P, Southworth S H, Young L and Keitel C H, *et al*. 2012 *Phys. Rev. A* **86** 033402
[28] Rohringer N and Santra R 2007 *Phys. Rev. A* **76** 033416
[29] Peyrusse O, Deschaud B and Rolles D 2014 *J. Phys. B: At. Mol. Opt. Phys.* **47** 011001
[30] Son S K and Santra R 2012 *Phys. Rev. A* **85** 063415
[31] Vartanyants I A, Singer A, Mancuso A P, *et al*. 2011 *Phys. Rev. Lett.* **107** 144801
[32] Lehmkühler F, Gutt C, Fischer B, Schroer M A, Sikorski M, Song S, Roseker W, Glownia J, Chollet M, Nelson S, Tono K, Katayama T, Yabashi M, Ishikawa T, Robert A and Grübel G 2014 *Sci. Rep.* **4** 5234
[33] Gao C, Zeng J L, Li Y Q, Jin F T and Yuan J M 2013 *High Energy Dens. Phys.* **9** 583
[34] Li Y, Krinsky S, Lewellen J W, Kim K J, Sajaev V and Milton S V 2003 *Phys. Rev. Lett.* **91** 243602
[35] Gu M F 2008 *Can. J. Phys.* **86** 675
[36] Li Y J, Liu L P, Gao C, Zeng J L and Yuan J M 2018 *J. Electron Spectrosc. Relat. Phenom.* **226** 26
[37] Müller A, Bernhardt D, Borovik A Jr., Buhr T, Hellhund J, Holste K, Kilcoyne A L D, Klumpp S, Martins M, Ricz S, Seltmann J, Viefhaus J and Schippers S 2017 *Astrophys. J.* **836** 166
[38] Oura M 2010 *Plasma Sci. Technol.* **12** 353
[39] Burke P G, Hibbert A and Robb W D 1971 *J. Phys. B: At. Mol. Opt. Phys.* **4** 153
[40] Berrington K A, Burke P G, Butler K, Seaton M J, Storey P J, Taylor K T and Yan Y 1987 *J. Phys. B: At. Mol. Opt. Phys.* **20** 6379
[41] Liu Y P, Zeng J L and Yuan J M 2013 *J. Phys. B: At. Mol. Opt. Phys.* **46** 145002
[42] Hibbert A 1975 *Comput. Phys. Commun.* **9** 141
[43] Pelicon P, Čadež I, Žitnik M, Šmit Ž, Dolenc S, Mühleisen A and Hall R I 2000 *Phys. Rev. A* **62** 022704
[44] Bhalla C P, Folland N O and Hein M A 1973 *Phys. Rev. A* **8** 649
[45] Karim K R and Logan L 1999 *J. Quant. Spectrosc. Radiat. Transfer* **61** 659
[46] Goldsztejn G, Marchenko T, Püttner R, Jornel L, Guillemin R, Carniato S, Selles P, Travnikova O, Céolin D, Lago A F, Feifel R, Lablanquie P, Piancastelli M N, Penent F and Simon M 2016 *Phys. Rev. Lett.* **117** 133001
[47] Deng P and Jiang G 2019 *Chin. Phys. B* **28** 063203
[48] Huang X C, Kong X J, Li T J, Ma Z R, Wang H C, Liu G C, Wang Z S, Li W B and Zhu L F 2021 *Phys. Rev. Res.* **3** 033063